frontiers in Earth Science

ORIGINAL RESEARCH
published: 29 November 2019
doi: 10.3389/feart.2019.00314

Pronounced Northwest African Monsoon Discharge During the Mid- to Late Holocene

Sebastian N. Höpker[1,2,3], Henry C. Wu[1]*, Peter Müller[1,4], Jean-Paul Barusseau[5], Robert Vernet[6], Friedrich Lucassen[7], Simone A. Kasemann[7] and Hildegard Westphal[1,2]*

[1] Leibniz Centre for Tropical Marine Research (ZMT) GmbH, Bremen, Germany, [2] Faculty of Geosciences, University of Bremen, Bremen, Germany, [3] Environmental Research Institute, School of Science, Faculty of Science and Engineering, University of Waikato, Hamilton, New Zealand, [4] BDG Berufsverband Deutscher Geowissenschaftler e.V., Bonn, Germany, [5] UMR 5110 Centre de Formation et de Recherche sur les Environnements Méditerranéens, University of Perpignan Via Domitia, Perpignan, France, [6] Institut Mauritanien de Recherches Scientifiques, Nouakchott, Mauritania, [7] Faculty of Geosciences and MARUM – Center for Marine Environmental Sciences, University of Bremen, Bremen, Germany

OPEN ACCESS

Edited by:
Michaël Hermoso, Université du Littoral Côte d'Opale, France

Reviewed by:
Anne-Marie Lezine, UMR 7159 Laboratoire d'Océanographie et du Climat Expérimentations et Approches Numériques (LOCEAN), France
Andrea Zerboni, University of Milan, Italy

***Correspondence:**
Sebastian N. Höpker
seb.hoepker@gmail.com
Henry C. Wu
henry.wu@leibniz-zmt.de

Specialty section:
This article was submitted to Quaternary Science, Geomorphology and Paleoenvironment, a section of the journal Frontiers in Earth Science

Received: *16 July 2019*
Accepted: *11 November 2019*
Published: *29 November 2019*

Citation:
Höpker SN, Wu HC, Müller P, Barusseau J-P, Vernet R, Lucassen F, Kasemann SA and Westphal H (2019) Pronounced Northwest African Monsoon Discharge During the Mid- to Late Holocene. Front. Earth Sci. 7:314. doi: 10.3389/feart.2019.00314

The mid- to late Holocene aridification pattern of NW Africa remains a matter of controversial debate. While many marine climate reconstructions indicate a relatively abrupt aridification at ~5.5 ka BP, terrestrial palaeoclimate records rather show a spatially and temporally heterogeneous transition towards the modern arid state. To bridge conflicting evidence, we analysed high-resolution (sub-seasonal) ontogenetic oxygen isotope ($\delta^{18}O$) records and bulk $^{87}Sr/^{86}Sr$ ratios of bivalve shells and fish otoliths of estuarine-associated species. Samples were excavated from archaeological deposits formed during the mid- to late Holocene in a large palaeo-estuary east of the Banc d'Arguin, Mauritania. The mid-Holocene (~5.2 ka BP) $\delta^{18}O$ records indicated unrealistically high water temperatures when assuming a modern value for $\delta^{18}O_{Seawater}$, suggesting a substantial input of isotopically lighter water to the study area. Respective salinity estimates consistently indicated persistent monsoonal discharge. Moreover, $^{87}Sr/^{86}Sr$ ratios of bivalve shells deviated considerably from the rather stable global seawater composition, further supporting the presence of significant terrestrial runoff between 5.0 and 5.3 ka BP. Altogether, our results support doubts regarding an abrupt termination of the African Humid Period (AHP) in the coastal areas of NW Africa, and show that fully marine conditions were established along the Banc d'Arguin by ~3.0 ka BP.

Keywords: African Humid Period, Mauritania, sclerochronology, bivalves, fish otoliths, archaeology, oxygen isotopes, $^{87}Sr/^{86}Sr$

INTRODUCTION

Previous studies consistently show that large parts of the present-day Sahara and Sahel region were dominated by dense savannah and shrub vegetation between ~15 and ~5 ka BP, the so-called African Humid Period (AHP) (Ritchie et al., 1985; deMenocal et al., 2000; Kuhlmann et al., 2004; Holz et al., 2007; Kröpelin et al., 2008; Roberts, 2014). During this period and several preceding humid episodes throughout the late Quaternary, increased Northern Hemisphere summer insolation induced a northward migration of the Intertropical Convergence Zone (ITCZ)

and the associated rain belt, and a significant intensification of the African monsoon. Across northern Africa, remnants of large palaeo-lakes and extensive fluvial networks illustrate the substantially altered hydroclimate during these periodic wet phases, which allowed for widespread human occupation of landscapes that are nowadays marked by (hyper)arid conditions with sparse or no vegetation (Kuper and Kröpelin, 2006). Enhanced monsoonal precipitation supplied a major drainage system covering much of modern Mauritania and the Arguin Basin during the AHP, with densely distributed archaeological shell midden deposits depicting numerous mid- to late Holocene settlements throughout the palaeo-estuary (Skonieczny et al., 2015) (**Figure 1**).

The exact timing and nature of the termination of the AHP and the transition to the modern arid state, however, remain a matter of considerable debate (Kröpelin et al., 2008; Claussen et al., 2013; Pausata et al., 2016). Many open marine dust records indicate an abrupt aridification around 5.5 ka BP, potentially triggered by bio-geophysical feedback mechanisms amplifying the gradually declining insolation during the mid- to late Holocene (deMenocal et al., 2000; Kuhlmann et al., 2004; McGee et al., 2013) (**Figures 2A,B**). Similarly, sedimentary leaf wax records from the Gulf of Guinea have recently been used to argue for a rapid termination of the AHP (Collins et al., 2017). The records ultimately linked the aridification to extratropical temperature changes and a non-linear response that resulted in the alteration of atmospheric circulation patterns. However, reconstructions of humidity and recent novel quantitative estimations of palaeo-precipitation using sediment cores retrieved off the coast of NW Africa depict a more gradual decrease in rainfall towards modern conditions (Tjallingii et al., 2008; Tierney et al., 2017) (**Figures 2C,D**). This is further supported by highly resolved dust records in a sediment core from the Mauritanian continental shelf (Hanebuth and Henrich, 2009). Various terrestrial and archaeological deposits from coastal settlements in turn suggest a spatially as well as temporally heterogeneous change in hydroclimate during the mid- to late Holocene (**Figure 2F**). These records provide evidence of a more gradual transition to the present-day arid state (Vernet and Tous, 2004; Vernet, 2007; Kröpelin et al., 2008; Armitage et al., 2015; Bloszies et al., 2015; Shanahan et al., 2015). Examples include several terrestrial and continental records from pollen-based reconstructions of hydroclimate and dendrochronology from the central Sahara that indicate spells of drought and regional progressive desertification (Cremaschi and Zerboni, 2009; Lézine, 2009; Lézine et al., 2011), which is further supported by palaeo-lake deposits, such as Lake Yoa in Chad (Lézine et al., 2011). Sea surface temperatures of the eastern tropical Atlantic remained relatively constant and were similar to modern values throughout the Holocene (Zhao et al., 1995; Kim et al., 2007) (**Figure 2E**), possibly punctuated by variable coastal upwelling intensities in response to changes in the trade wind regimes (Talbot, 1981; Romero et al., 2008; Hély et al., 2014).

Considering the conflicting evidence from different proxy records, climate model simulations increasingly fail to reproduce the suggested abruptness of the mid-Holocene climate transition (Liu et al., 2007; Rachmayani et al., 2015; Shanahan et al., 2015; Pausata et al., 2016), and strongly underestimate reconstructed precipitation rates over NW Africa (Tierney et al., 2017). A number of studies have further noted that interpretations of different proxy systems, even within the same archive, may inherently lead to contrasting conclusions given the varying nature of the respective environmental controls (Castañeda et al., 2016). In consequence, we are still lacking a holistic understanding of the temporal and spatial aridification pattern of NW Africa during the Holocene, and subsequently of the underlying mechanisms governing the intensity and spatial extent of the West African Monsoon. This in turn prohibits reliable predictions regarding the response of the West African climate to future global changes.

In this study, we use oxygen isotope ($\delta^{18}O$) records of modern and archaeological bivalve shells (*Senilia senilis*) and catfish otoliths (*Carlarius* spp.) from the Banc d'Arguin, Mauritania, to complement conflicting evidence from marine and terrestrial proxy archives, and provide further information on the timing of the Holocene termination of monsoonal precipitation. Sub-seasonally resolved $\delta^{18}O$ records of both *S. senilis* shells and catfish otoliths have previously been shown to reliably trace environmental conditions, allowing for water temperature estimates with absolute uncertainties of $\leq 1.5°C$ (Surge and Walker, 2005; Lavaud et al., 2013; Müller et al., 2015). Variable growth patterns throughout the organisms' lifetimes, however, hamper a straightforward conversion of ontogenetic data from incrementally banded skeletal structures into time series of environmental parameters, such as temperature or salinity (Goodwin et al., 2003). In the absence of a standardised method, a vast range of approaches has been used to align biological proxy records with instrumental data. However, many methods are not readily traceable and consequently lack reproducibility to assess their reliability. To this effect, we used a linear interpolation technique developed by Müller et al. (2015), where the proxy records are mathematically aligned with environmental data via carefully determined temporal reference points. This method has been shown to allow for a flexible and transparent establishment of temporal frameworks for sclerochronological records that also accommodates for growth variations (Müller et al., 2015).

Given the association of the studied taxa with estuarine environments, their ontogenetic $\delta^{18}O$ signatures are predicted to be influenced by freshwater discharge with strong negative excursions in ambient $\delta^{18}O_{Water}$ values reflecting the drainage of isotopically lighter monsoon precipitation (Surge and Walker, 2005; Azzoug et al., 2012a,b). Therefore, ontogenetic $\delta^{18}O$ records are expected to show combined signals of seasonal water temperature and freshwater discharge during times of increased riverine input into the coastal zone of the Banc d'Arguin. Considering observations of relatively constant water temperatures in coastal NW Africa throughout the Holocene (Zhao et al., 1995; Kim et al., 2007), a disentangling of these combined signals is possible with the resulting $\delta^{18}O$-based salinity reconstructions expected to depict brackish conditions. Moreover, $\delta^{18}O$ records of specimen subject to monsoonal activity are expected to show generally more pronounced seasonal signals.

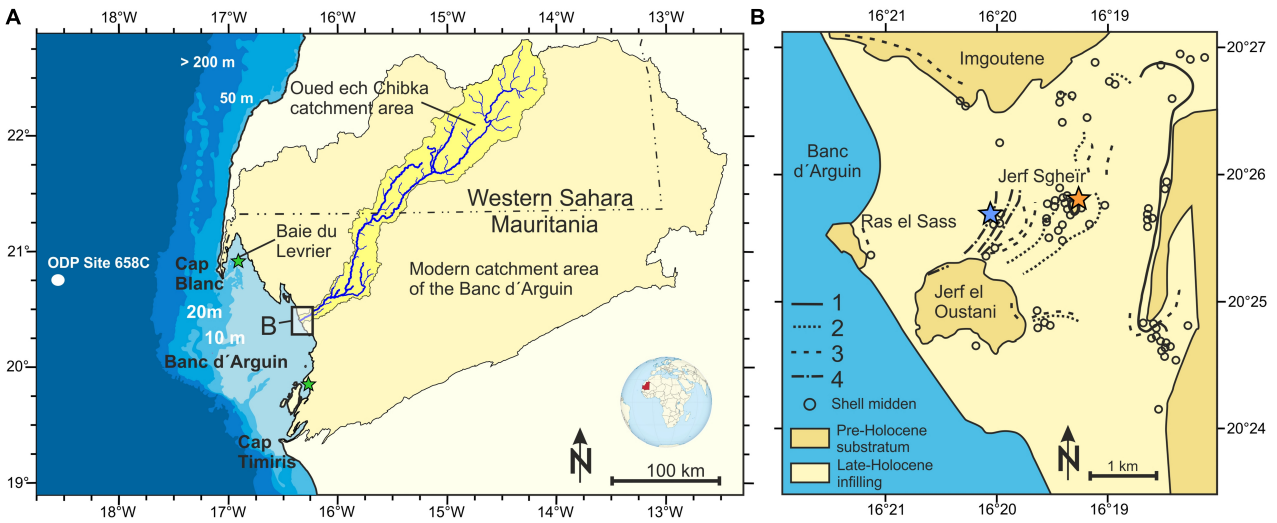


FIGURE 1 | Research area at Banc d'Arguin, Mauritania, NW Africa. **(A)** NW African coastline bathymetry with the shallow Banc d'Arguin, and the modern catchment area draining into the Banc d'Arguin. Approximate sample locations of modern catfish otoliths (Baie du Lévrier) and bivalve shells (near Iwik, southern part of the Banc d'Arguin; see Lavaud et al., 2013 for details) are indicated by green stars. **(B)** Close-up of the study site in the hinterland of Ras el Sass in the mouth of a large palaeo-estuary (Skonieczny et al., 2015). The location of shell midden alignments and beach ridges show the human occupation pattern following the coastal progradation throughout the mid- to late Holocene: 1: > 5000 years BP according to archaeological evidence; 2: Jerf Sgheïr shell midden of this study (5320–5020 years BP); 3: Tintan group (4600–4000 years BP); 4: Last Neolithic groups (3300 years BP). Archaeological ages adapted from Barusseau et al. (2007). Approximate locations of mid-Holocene and late Holocene samples are indicated by orange and blue markers, respectively. The map and inlet map were created using the SRTM 1 Arc-Second (USGS, 2004) dataset (available at https://earthexplorer.usgs.gov/). The catchment area in **A** was calculated using the SCALGO Live Global online platform (www.scalgo.com/live) based on World HydroSHEDS (Lehner et al., 2008, available at http://www.hydrosheds.org/). Maps were modified manually.

When using geochemical proxies from archaeological midden constituents, however, a potential alteration of the sample material due to pre-depositional cooking treatments needs to be considered. For instance, heating has been shown to potentially induce mineralogical phase changes (e.g. Andrus and Crowe, 2002; Milano and Nehrke, 2018) and/or microstructural alterations (e.g. Maritan et al., 2007; Cremaschi et al., 2015). Moreover, the original $\delta^{18}O$ signatures of skeletal aragonite can evidently be altered when subjected to prehistoric cooking methods, which may lead to considerable errors in palaeoenvironmental reconstructions (Andrus and Crowe, 2002; Milano et al., 2016; Müller et al., 2017). In this study, we use carbonate clumped isotope thermometry to evaluate the preservation state and reliability of proxy interpretations of samples used in this study. This method has recently been demonstrated as a valuable tool to detect and quantify such potential bias based on the temperature-dependent re-equilibration of clumped isotopes in aragonite (Müller et al., 2017).

To further support the ontogenetic $\delta^{18}O$ records, we present bulk strontium isotope ratios ($^{87}Sr/^{86}Sr$) from the two skeletal materials as an additional indicator for freshwater influx. $^{87}Sr/^{86}Sr$ signatures in biogenic carbonates effectively reflect the Sr isotopic composition of the ambient water during the incorporation of strontium into the carbonate structure due to the lack of any significant mass fractionation (Palmer and Edmond, 1989). Given the long residence time of Sr in the ocean, $^{87}Sr/^{86}Sr$ values of seawater are globally highly consistent [ca. 0.70918 ± 0.00001; two standard deviations (SD)] (Faure and Mensing, 2005) and have remained essentially constant over the past ~40 ka (Mokadem et al., 2015). Sr isotope signatures of riverine water are in turn primarily governed by the respective catchment geology, and are typically considerably different to those observed in seawater. While there is no modern freshwater influx available as reference along the Mauritanian coast, measurements of hinterland dust sources and sediments derived from granitic bedrock located in the palaeo-drainage area to the Banc d'Arguin consistently indicate more radiogenic $^{87}Sr/^{86}Sr$ values than those of seawater of up to 0.74 (e.g. Scheuvens et al., 2013; Zhao et al., 2018). Since Sr concentrations of seawater (ca. 7.74 ppm) are typically one to two magnitudes higher than those observed in average river water (Faure and Mensing, 2005), a pronounced deviation from the marine end-member in bulk otolith or bivalve samples is expected to reflect an influx of substantial volumes of riverine discharge to the organisms' habitat over their lifetime.

MATERIALS AND METHODS

Sample Material and Background

Modern sea catfish (*Carlarius parkii* and *Carlarius heudelotii*) otoliths were extracted from individuals caught by local fishermen in the central Baie du Lévrier in November 2011 (Müller et al., 2015) and in March 2012 (this study). Modern

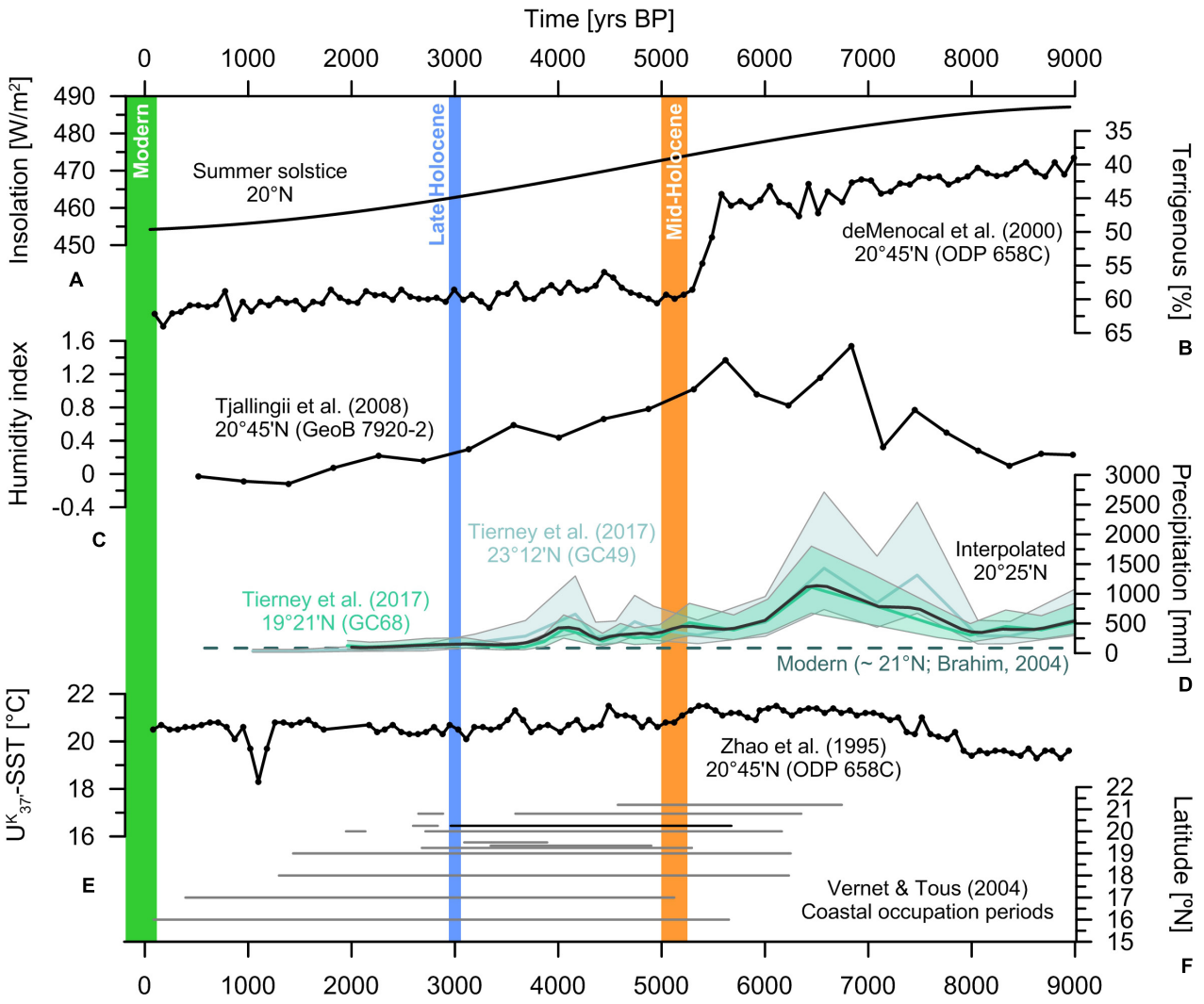


FIGURE 2 | Palaeoclimate records of NW Africa. **(A)** Summer (solstice) insolation at 20°N (Laskar et al., 2004). **(B)** Terrestrial dust export at ODP site 658C (deMenocal et al., 2000). **(C)** Continental humidity index based on grain-size measurements of GeoB 7920-2 (Tjallingii et al., 2008). **(D)** δD-based precipitation reconstruction (Tierney et al., 2017) with a temporal and spatial interpolation at 20°25°N and the modern annual precipitation at ~21°N (Brahim, 2004). **(E)** Holocene alkenone water temperature record from ODP site 658C (Zhao et al., 1995). **(F)** Periods of coastal occupation along the West African coast (Vernet and Tous, 2004). The Ras el Sass area is marked in black. Time periods covered by sample material discussed in this study are shown as green, blue, and orange columns for the modern (2010–2012 AD), late Holocene (ca. 3.0 ka BP), and mid-Holocene (ca. 5.3–5.0 ka BP), respectively.

bivalves (*S. senilis*) were originally assessed in Lavaud et al. (2013) and used for additional analyses herein.

The archaeological samples were excavated from a succession of shell midden deposits in the vicinity of the palaeo-island Jerf Sgheïr in the Ras el Sass area, Mauritania, NW Africa (**Figure 1** and **Supplementary Figure S1**, see Barusseau et al., 2007 for details on archaeological deposits in this region). The mid-Holocene otoliths and bivalve shells were previously discussed in Müller et al. (2017) regarding potential alterations due to pre-depositional cooking treatments, and are further analysed in this study. In addition, data from two late Holocene *Carlarius* spp. otoliths from the same study site that were prepared for analyses following the procedure described in Müller et al. (2017) are presented. An overview of samples used in this study can be found in **Table 1**. All otoliths and bivalve shells were ultrasonically cleaned in deionised water, and carefully dried at 30 °C for 48 h. The outermost layers of bivalve shells and otoliths were manually removed using a Dremel® tool to exclude potential surficial contamination.

Mineralogical Analysis and Radiocarbon Dating

The mineralogy of the two late Holocene otoliths was assessed using a Philips X'Pert Pro diffractometer equipped with a Cu-tube (kα 1.541, 45 kV, 40.0 mA) at the University of Bremen, Germany. A continuous scan from 3–85° 2θ with a step size of 0.016° 2θ was carried out, and data were processed using the Philips

TABLE 1 | Mauritanian bivalve shells and fish otoliths used in this study.

Material	Sample ID	Organism	Location	First published
Fish otolith	RAH1	*Carlarius heudelotii*	Baie du Lévrier	Müller et al. (2015)
Fish otolith	RAP1	*Carlarius parkii*	Baie du Lévrier	This study
Bivalve shell	#3009	*Senilia senilis*	Iwik	Lavaud et al. (2013)
	#3122			
	#3211			
Fish otolith	OTO-B5 OTO-B6	*Carlarius* spp.	Jerf Sgheïr 20°25'37"N 16°19'34"W	This study
Fish otolith	OTO-B3	*Carlarius* spp.	Jerf Sgheïr 20°25'37"N 16°19'34"W	Müller et al. (2017)
	OTO-B4			
	OTO-B8			
	OTO-B9			
Bivalve shell	JS-SS-1	*Senilia senilis*	Jerf Sgheïr 20°25'37"N 16°19'34"W	Müller et al. (2017)
	JS-SS-2			
	JS-SS-3			
	JS-SS-4			
	JS-SS-5			
	JS-SS-6			
	JS-SS-10			

software X'Pert HighScore™. Aragonite and calcite abundances were determined based on the relative peak areas of aragonite (1,1,1; peak at $2\theta = 26.1°$) and low-Mg calcite (1,0,1; peak at $2\theta = 29.6°$) against calibrated standard material.

Radiocarbon dating of the two otoliths was carried out at the Poznań Radiocarbon Laboratory, Poznań, Poland, following standard procedures for accelerator mass spectrometry. Conventional radiocarbon ages were calibrated with OxCal 4.3 (Bronk Ramsey, 1995) using the Marine13 calibration curve (Reimer et al., 2013), and assuming a local reservoir age of $\Delta R = -300$ years (Müller et al., 2017). This value of ΔR presents an estimated average for the mid- to late Holocene based on various paired radiocarbon dates from terrestrial and marine materials (Saliège, unpublished). Mineralogical data and radiocarbon ages of samples used in this study are compiled in **Table 2**.

Ontogenetic $\delta^{18}O$ Analyses of Modern and Holocene Samples

The preparation of otolith and bivalve shell thick and thin sections, and ontogenetic sub-sampling for $\delta^{18}O$ analysis were completed at the Leibniz Centre for Tropical Marine Research (ZMT), Bremen, Germany, as described in detail in Müller et al. (2015). Otolith thick sections were drilled using a Merchantec® Micromill equipped with a 150 μm diameter drill bit from the edge of the otolith towards the core with a spacing between samples of ca. 100 μm, yielding between 47 and 57 discrete sub-samples. Thick sections of bivalve shells were used to sample along the outer shell layer from the hinge towards the ventral margin with average spacing of ca. 500 μm, which resulted in 35–61 discrete sub-samples per shell.

The $\delta^{18}O$ values of individual otolith and shell sub-samples (∼50 μg) were determined using a Finnigan MAT 251 gas isotope ratio mass spectrometer (IRMS) connected to a Kiel III device at the MARUM – Center for Marine Environmental Sciences, University of Bremen, Germany, and a Thermo Finnigan MAT 253 IRMS connected to a Kiel IV device at the Leibniz Centre for Tropical Marine Research (ZMT), Bremen, Germany. Repeated standard measurements (NBS 19 and in-house working standards) revealed an external precision (1SD) for all measurements of better than ±0.07‰ for all $\delta^{18}O$ analyses.

Temporal Alignment of Ontogenetic $\delta^{18}O$ Records

In order to produce sub-seasonally resolved reconstructions of Holocene water temperatures and salinities, the ontogenetic otolith and bivalve $\delta^{18}O$ records (**Supplementary Figures S2**, **S3**) were converted into time series using the linear interpolation approach of Müller et al. (2015), and SST records for the Banc d'Arguin (see **Supplementary Figures S4**, **S5** and the **Supplementary Material** for details on the temporal alignment and interpolation approach). The linear interpolation model for the temporal alignment assumed a sinusoidal growth oscillation and winter growth cessations. The potential absolute uncertainty of linear interpolation models was estimated to be ca. 1.15°C based on mean absolute errors (MAEs) between $\delta^{18}O$-based reconstructed water temperatures from modern bivalves and observed SSTs in the Banc d'Arguin (a detailed description of the error estimation can be found in the **Supplementary Material**).

Ontogenetic $\delta^{18}O$ Records-Based Temperature and Salinity Reconstructions

Modern and Holocene water temperatures were reconstructed using the equation of Thorrold et al. (1997) for the fish otoliths, and the equation of Grossman and Ku (1986) for the bivalve shells assuming a constant $\delta^{18}O_{Seawater}$ composition of +0.68‰ (Müller et al., 2015) and +1.57‰ VSMOW (Lavaud et al., 2013), respectively. These newly established ontogenetic $\delta^{18}O$ datasets were combined with previously published $\delta^{18}O$ records of a modern catfish otolith (*C. heudelotii* from Müller et al., 2015), three modern bivalve shells (*S. senilis* from Lavaud et al., 2013) and three mid-Holocene bivalve shells (*S. senilis* from Müller et al., 2017).

For subsequent reconstructions of modern and Holocene (palaeo-) salinities, we assumed that the mid- to late Holocene water temperatures were similar to the modern values, which has been shown in several previous studies for the eastern tropical Atlantic (Zhao et al., 1995; Kim et al., 2007). Ontogenetic $\delta^{18}O_{Water}$ values were calculated based on the measured

TABLE 2 | Clumped isotope, mineralogy and radiocarbon data of the modern and Holocene specimens.

Sample	Species	Δ_{47} (‰, ARF)	SE (±) (‰, ARF)	Aragonite (wgt %)	Calcite (wgt %)	^{14}C age (years BP)	Uncertainty (± years)	ΔR (years)	Cal. years BP from	Cal. years BP to	Median	Uncertainty + (years)	Uncertainty – (years)
RAP-1	*C. parkii*	–	–	100	0	Modern	–	–	–	–	–	–	–
RAH-1	*C. heudelotii*	–	–	98	2	Modern	–	–	–	–	–	–	–
Late Holocene otoliths													
OTO-B5	*Carlarius* spp.	0.668	0.013	100	0	3170	40	–300	3100	2830	2960	140	130
OTO-B6	*Carlarius* spp.	0.691	0.014	–	–	3250	30	–300	3180	2950	3070	110	110
Mid-Holocene otoliths													
OTO-B3	*Carlarius* spp.	0.716	0.013	100	0	4920	30	–300	5330	5070	5260	70	190
OTO-B4	*Carlarius* spp.	0.714	0.011	95	5	4970	30	–300	5430	5250	5320	110	70
OTO-B8	*Carlarius* spp.	0.704	0.014	100	0	4920	35	–300	5390	5260	5260	130	200
OTO-B9	*Carlarius* spp.	0.667	0.016	100	0	4970	35	–300	5440	5320	5320	120	80
Mid-Holocene bivalves													
JS-SS-1	*S. senilis*	0.666	0.014	100	0	4830	35	–300	5270	4990	5130	140	140
JS-SS-2	*S. senilis*	0.601	0.014	100	0	4770	35	–300	5210	4880	5020	190	140
JS-SS-3	*S. senilis*	0.667	0.013	100	0	4845	35	–300	5280	4020	5150	130	130
JS-SS-4	*S. senilis*	0.631	0.012	100	0	–	–	–	–	–	–	–	–
JS-SS-5	*S. senilis*	0.661	0.013	100	0	–	–	–	–	–	–	–	–
JS-SS-6	*S. senilis*	0.716	0.013	100	0	–	–	–	–	–	–	–	–
JS-SS-10	*S. senilis*	0.622	0.017	100	0	–	–	–	–	–	–	–	–

Clumped isotope analyses were performed at the Stable Isotope Laboratory (SIL) at the Rosenstiel School of Marine and Atmospheric Science (RSMAS) of the University of Miami, FL, United States, following the protocol previously described in detail in Müller et al. (2017). Mineralogical analyses were performed at the University of Bremen, Germany. Radiocarbon dating was done at the Poznań Radiocarbon Laboratory, Poland. Radiocarbon ages were calibrated using OxCal 4.3 (Bronk Ramsey, 1995) with the Marine13 calibration curve (Reimer et al., 2013) and a local ΔR value of -300 years (Müller et al., 2017).

ontogenetic $\delta^{18}O_{Carbonate}$ values and corresponding interpolated SSTs after the temporal alignment of individual $\delta^{18}O$ records with the averaged SST time series. For the fish otoliths, we used the equation of Thorrold et al. (1997):

$$10^3 \ln \alpha = 18.56 \cdot \left(10^3 \cdot T^{-1}[K]\right) - 32.54$$

with

$$\alpha = \frac{\delta_{Aragonite} + 10^3}{\delta_{Water} + 10^3}$$

The conversion from the VPDB into the VSMOW scale was done using the equation of Gonfiantini et al. (1995) defined as:

$$\delta^{18}O\ [VSMOW] = 1.03091 * \delta^{18}O\ [VPDB] + 30.91$$

For the calculation of $\delta^{18}O_{Water}$ values from the bivalve shell $\delta^{18}O$ records, we used the equation of Grossman and Ku (1986) in the same form as used by Lavaud et al. (2013):

$$T\ [^{\circ}C] = 21.8 - 4.69 \cdot \left(\delta^{18}O_{Aragonite\ [VPDB]} - (\delta^{18}O_{Seawater\ [VSMOW]} - 0.27)\right)$$

For the modern fish otoliths and bivalve shells, the resulting $\delta^{18}O_{Seawater}$ time series were transformed into salinity time series using a linear mixing model based on modern marine and freshwater end-members. For the approximation of the modern and Holocene marine end-members, we used the local $\delta^{18}O_{Water}$-salinity model of Lavaud et al. (2013) following the equation:

$$\delta^{18}O_{Seawater}\ [VSMOW] = 0.2692 * Salinity - 9.1949$$

and the average SODA sea surface salinity (Carton and Giese, 2008) with a spatial coverage of 1° by 1° (20–21°N, 16–17°W) of the Banc d'Arguin averaged over a 10-year period (1999–2009) resulting in a marine end-member with a salinity of 36.69 and a $\delta^{18}O_{Seawater}$ value of 0.68‰ VSMOW. For the modern freshwater end-member, we used a modelled $\delta^{18}O_{Precpitation}$ value representative of the Mauritanian hinterland (salinity = 0, $\delta^{18}O_{Precpitation}$ = -3.35‰ VSMOW) obtained using the OIPC (Bowen and Revenaugh, 2003; Bowen, 2015; IAEA/WMO, 2015) (Ver. 2.2., available at wateriso.utah.edu/waterisotopes).

For the late Holocene, we used the same marine end-member, and the freshwater end-member (i.e. $\delta^{18}O_{Precpitation}$) has been approximated based on spatially and temporally interpolated δD data from Tierney et al. (2017) and the equation of Craig (1961):

$$\delta D\ [VSMOW = 8 \cdot \delta^{18}O\ [VSMOW] + 10$$

We used the δD records of sediment cores GC49 (23.206°N) and GC68 (19.363°N) by Tierney et al. (2017) and associated age models to interpolate the δD values at 20.417°N (Jerf Sgheïr shell midden successions) in 100 year intervals. This calculation resulted in a late Holocene $\delta^{18}O_{Precpitation}$ value of −3.45‰ VSMOW, which is similar to the modern value. For the mid-Holocene, the same approach resulted in a freshwater end-member with a $\delta^{18}O_{Precpitation}$ value of −4.25‰ VSMOW.

The combined absolute uncertainty of the $\delta^{18}O_{Carbonate}$-based salinity reconstructions was approximated by combining the average MAE resulting from the temporal alignment of the modern *S. senilis* shells with averaged OI-SST data (±1.15°C, translating into a salinity error of ±2.21 practical salinity units; S_p) with the uncertainty of mid- to late Holocene water temperature reconstructions (±1°C, translating into a salinity error of 1.92 S_p). This error estimation resulted in a total absolute uncertainty of the salinity reconstruction of ±4.13 S_p.

Sr-Isotope ($^{87}Sr/^{86}Sr$) Analysis

Strontium isotope ratios of bulk bivalve and otolith samples (i.e. material representing the entire lifespan of each individual) were determined by using a Thermo Scientific Triton Plus thermal ionisation mass spectrometer (TIMS) in the Isotope Geochemistry Laboratory at MARUM, Bremen, Germany. Approximately 2 mg of homogenised carbonate powder were dissolved in 2 M HNO_3, dried and re-dissolved in 500 µl of 2 M HNO_3 in preparation for the chemical separation of Sr from unwanted matrix elements. Following a setup and procedure adapted from Deniel and Pin (2001), Sr was extracted using miniature columns loaded with ca. 70 µl of Sr-spec ion exchange resin (Eichrom Technologies, LLC, United States). The collected Sr was loaded on single Re filaments with Ta-oxide emitter, and analysed by TIMS using a multidynamic acquisition routine. All $^{87}Sr/^{86}Sr$ ratios were normalised to a $^{86}Sr/^{88}Sr$ ratio of 0.11940 to correct for instrumental mass fractionation. The long-term external instrumental reproducibility with respect to NIST 987 standard material is 0.710249 ± 0.000014 (2SD, n = 263).

Clumped Isotope Analysis

The powdered bulk skeletal samples were analysed for clumped isotopes to assess for potential alterations due to pre-depositional cooking treatments (Andrus and Crowe, 2002; Müller et al., 2017). The mid-Holocene samples were previously presented and detailed in Müller et al. (2017) (**Table 2**). Clumped isotope analysis of the late Holocene otolith samples followed established methodology presented in Müller et al. (2017) and was completed at the Stable Isotope Laboratory of the Rosenstiel School of Marine and Atmospheric Science (RSMAS), University of Miami, Miami, FL, United States. Data reduction, normalisation for Δ_{47} and temperature calculations were carried out as previously described in Affek and Eiler (2006) and Huntington et al. (2009). The external instrumental precision (presented as average standard errors of individual measurements) was determined by repeated measurements of a Carrara marble (mean Δ_{47} = 0.4001 ± 0.0294‰; n = 191). Translation into the absolute reference frame (ARF) with 1000, 50 and 25°C water equilibrated gasses was completed with the method of Dennis et al. (2011).

RESULTS

To assess mid- to late Holocene changes in monsoonal discharge in NW Africa, we analysed modern and archaeological catfish otoliths and bivalve shells from the Banc d'Arguin, Mauritania (see **Table 1** for an overview of samples).

The preservation state of all fossil carbonate samples was assessed via X-ray diffraction (XRD) and thin section microscopy, both of which indicate near pristine conditions comparable to those of modern equivalents. XRD measurements suggest very good preservation of the initial primarily aragonitic mineralogy and calcite fractions ranging from the undetectable to less than 2%, with the exception of OTO-B4 (indicating ca. 5% calcite, **Table 2**). Microstructure analysis by scanning electron microscope (SEM) of samples used confirms the structural integrity and does not show any evidence for internal cementation or re-mineralisation (see **Supplementary Figure S6** for exemplary images). Given their archaeological origin, we assessed the Holocene samples for any potential alteration related to prehistoric cooking practices using clumped isotope thermometry. Both late Holocene otolith Δ_{47} values range from 0.668 to 0.691‰, consistent in magnitude with the mid-Holocene otoliths (0.667–0.714‰) reported in Müller et al. (2017), placing them within the limits of potential minor alterations (**Figure 3** and **Table 2**). In line with recent experimental evidence indicating that radiocarbon is not sensitive to heating induced in cooking practices (Lindauer et al., 2018), we accept our ^{14}C ages to be reliable.

The ontogenetic $\delta^{18}O$ records of all carbonate samples show a pronounced seasonality with clear sinusoidal patterns (**Supplementary Figures S2**, **S3**). Similar to the *C. heudelotii* otolith $\delta^{18}O$ record from Müller et al. (2015), the $\delta^{18}O$ record of the modern *C. parkii* otolith RAP-1 varies between −0.45 and +1.47‰ VPDB with an average $\delta^{18}O_{Carbonate}$ composition of +0.17‰ VPDB (**Figure 4A** and **Supplementary Figures S2**, **S4**). Assuming a constant $\delta^{18}O_{Seawater}$ of +0.68‰ VSMOW, these values translate into water temperatures ranging from 18.0 to 27.1°C with an average value of 24.1°C (**Figure 4B** and **Supplementary Figures S2**, **S4**).

Ontogenetic $\delta^{18}O$ records of the late Holocene *Carlarius* spp. otoliths exhibit a similar range between −0.59 and +2.03‰ VPDB with average values of +0.80 and +0.35‰ VPDB, translating into water temperatures ranging from 15.5 to 27.8°C with average values of 21.1 and 23.3°C (**Figure 4B** and **Supplementary Figures S2**, **S4**).

Mid-Holocene otoliths also show pronounced seasonal cycles within their ontogenetic $\delta^{18}O$ records (**Supplementary Figure S2**). However, their $\delta^{18}O_{Carbonate}$ values are considerably lower than their modern and late Holocene equivalents, varying between −2.61 and +1.18‰ VPDB with average values from −0.94 to −0.14‰ VPDB. These $\delta^{18}O_{Carbonate}$ values translate into reconstructed water temperatures ranging from 19.4 to 37.9°C and average values between 25.6 and 29.5°C (**Figure 4B**). The average seasonal minimum and maximum water temperature based on the mid-Holocene otolith samples was found to be 21.4 and 34.7°C.

The $\delta^{18}O$ records of mid-Holocene *S. senilis* shells show minimal and maximal values of −3.33 and +1.68‰ VPDB (**Supplementary Figure S3**). Assuming a constant $\delta^{18}O_{Seawater}$ value of +1.57‰ VSMOW, these values suggest ambient water temperatures between 20.0 and 43.5°C (**Figure 4B**).

To assess temporal differences in the seasonality amongst samples, we further established the mean seasonal amplitude of each ontogenetic $\delta^{18}O$ record. For consistency and robustness, we computed the averages of all clearly distinguishable local maxima and all local minima as observed in the raw ontogenetic $\delta^{18}O$ records of each sample (see **Supplementary Figures S2**, **S3**). The seasonal amplitude was estimated as the difference between mean maxima and minima, accordingly, while the range of all ontogenetic $\delta^{18}O$ values was considered in addition (**Figure 5**, c.f. Bougeois et al., 2014). For modern bivalve shells, the mean seasonal amplitude was found to be ca. 2.0‰, slightly higher than observed in modern catfish otoliths (ca. 1.4‰). In comparison, the late Holocene otolith OTO-B5 exhibits a distinctly higher amplitude, whereas OTO-B6 is consistent with the modern average. In contrast, all mid-Holocene otoliths show amplitudes higher than their modern equivalents. Mid-Holocene bivalve shells show variable seasonal amplitudes compared to the modern average, with many sample records exhibiting a large internal variability. The ranges of most of their ontogenetic records are noticeably higher than those of their modern equivalents. Similarly, mid-Holocene otoliths show ranges consistently greater than those in modern specimen, whereas late Holocene otoliths are coherent with modern samples.

To further constrain the potential influence of isotopically lighter freshwater runoff, we used the ontogenetic $\delta^{18}O$ records to reconstruct salinity under the assumption that water temperatures were similar during the mid-Holocene as observed today. We aligned all ontogenetic $\delta^{18}O$ records to averaged modern water temperature time series (**Supplementary Figures S4**, **S5**) and approximated $\delta^{18}O_{Water}$ values. Salinities were subsequently estimated using different $\delta^{18}O_{Water}$-salinity models (**Figure 6**). We used modelled modern $\delta^{18}O_{Precipitation}$ obtained using the Online Isotopes in Precipitation Calculator (Bowen and Revenaugh, 2003; Bowen, 2015; IAEA/WMO, 2015) (OIPC, Ver. 2.2, available at wateriso.utah.edu/waterisotopes) and sediment core-based δD-data from Tierney et al. (2017) for the approximation of Holocene $\delta^{18}O_{Precipitation}$ (**Figure 6**). Using this approach, the modern average reconstructed salinities are in very good agreement with the measured values ∼36 S_p for the fish otoliths (Müller et al., 2015) and ∼40 S_p for the *S. senilis* shells (Lavaud et al., 2013) (**Figures 4C**, **6**). The late Holocene otoliths also show purely marine conditions with salinities varying around the modern value of ∼36 S_p. In contrast, mid-Holocene salinity reconstructions indicate consistently brackish to marine conditions within the coastal zones with average salinities ranges of 25.7–31.8 S_p and 27.5–34.1 S_p for the catfish otoliths and the bivalve shells, respectively (**Figure 4C**).

$^{87}Sr/^{86}Sr$ ratios of all mid-Holocene bivalve samples are considerably higher than the marine end-member of 0.70918 (**Figure 4D**) with averages ranging from ca. 0.70928 to 0.70934. The $^{87}Sr/^{86}Sr$ ratios are highly consistent amongst different bivalve samples. In otoliths, the mid-Holocene $^{87}Sr/^{86}Sr$ ratios range from ca. 0.70921 to 0.70924, whereas those of late Holocene specimens are coherent with seawater (**Figure 4D**). The modern catfish otoliths, in contrast, exhibit considerable deviations from the seawater end-member as well as among samples, with relatively radiogenic $^{87}Sr/^{86}Sr$ ratios of up to ca. 0.70929, similar to those observed in mid-Holocene bivalve shells.

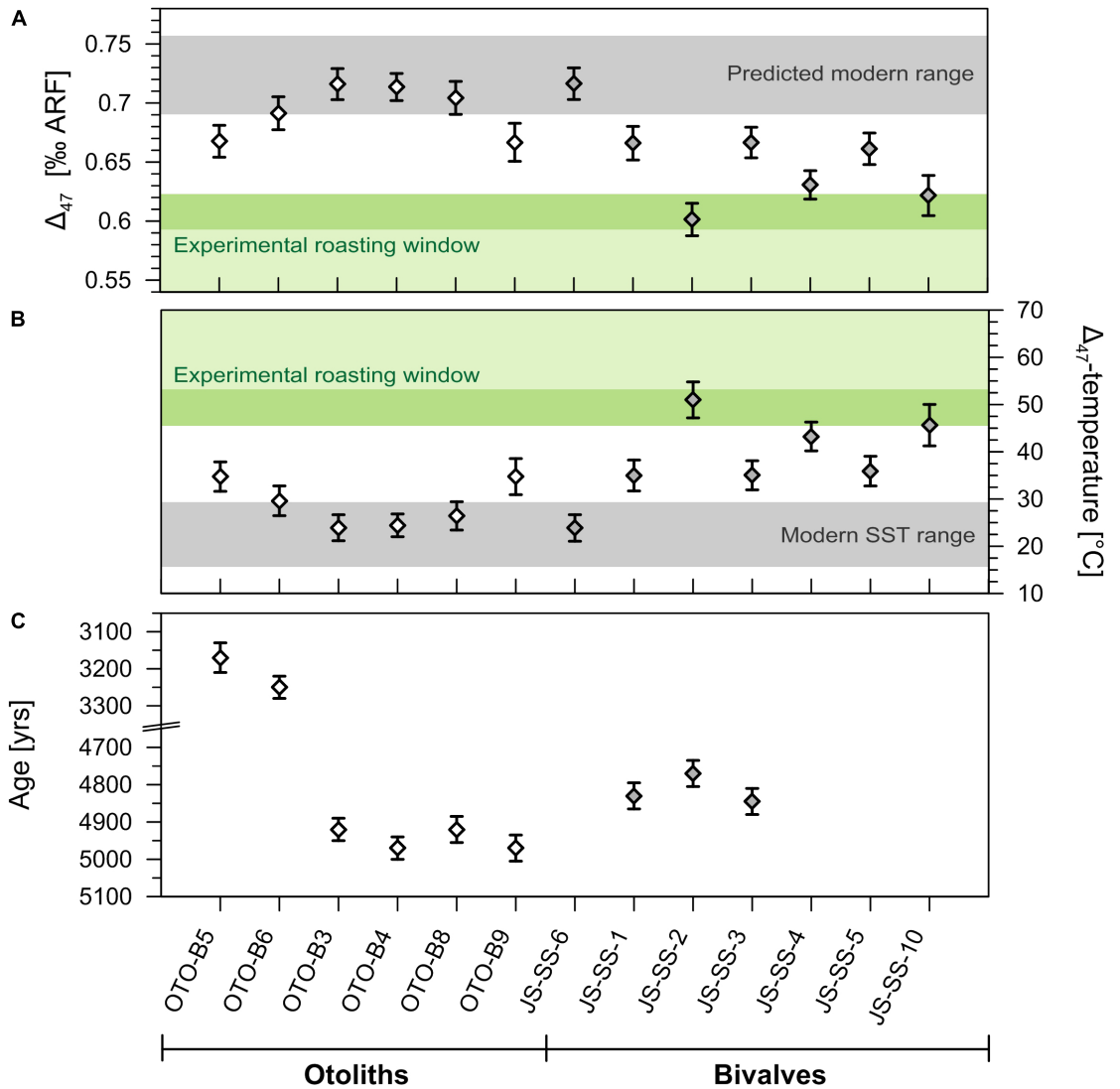


FIGURE 3 | Clumped isotope geochemistry and radiocarbon ages of Holocene specimens. **(A)** Clumped isotope data of the Holocene otoliths and bivalve shells. Mid-Holocene samples have previously been discussed in Müller et al. (2017). **(B)** Δ_{47}-based water temperatures estimated using the equation of Dennis et al. (2011). Error bars represent average standard errors (SE) of the individual Δ_{47}-measurements. The shaded grey areas represent predicted Δ_{47}-values in **A** based on the seasonal SST range from Lavaud et al. (2013) shown in **B**. Shaded green areas represent the experimental Δ_{47}-/temperature windows for prehistoric cooking (roasting at ca. 174°C) from Müller et al. (2017) for ca. 6 h (light green) and a more realistic cooking duration of > 30 min (dark green). Only very few mid-Holocene shells exhibit Δ_{47} values that suggest a potential alteration due to prehistoric cooking practices (roasting), whereas fish otoliths show little indication of significant pre-depositional heating. **(C)** Radiocarbon ages were calibrated using OxCal 4.3 (Bronk Ramsey, 1995) with the Marine13 calibration curve (Reimer et al., 2013) and a local ΔR value of −300 years (Müller et al., 2017).

DISCUSSION

The key findings of our study are based on the oxygen and strontium isotope records of archaeological bivalve shells and catfish otoliths from the Banc d'Arguin, Mauritania, which collectively provide strong evidence of significant freshwater discharge to the region between ca. 5.3 and 5.0 ka BP. Importantly, our data thereby contradict existing datasets derived from marine sediment cores off the Mauritanian coast, which indicate an abrupt cease of pronounced precipitation across NW Africa by about 5.5 ka BP (deMenocal et al., 2000).

As a modern reference for our reconstructions of water temperature and salinity, we established new ontogenetic $\delta^{18}O$ records of a *C. parkii* otolith, RAP-1, which are consistent in their seasonal cyclicity and magnitude with the *C. heudelotii* otolith $\delta^{18}O$ record from Müller et al. (2015). Both otolith $\delta^{18}O$ signatures yield water temperature estimates that are in good agreement with the modern seasonal water temperature amplitude on the Banc d'Arguin (**Figure 2E**). Despite possible discrepancies between reconstructed and recorded SSTs, ontogenetic $\delta^{18}O$ records of both catfish species occurring on the Banc d'Arguin (*C. heudelotii* and *C. parkii*),

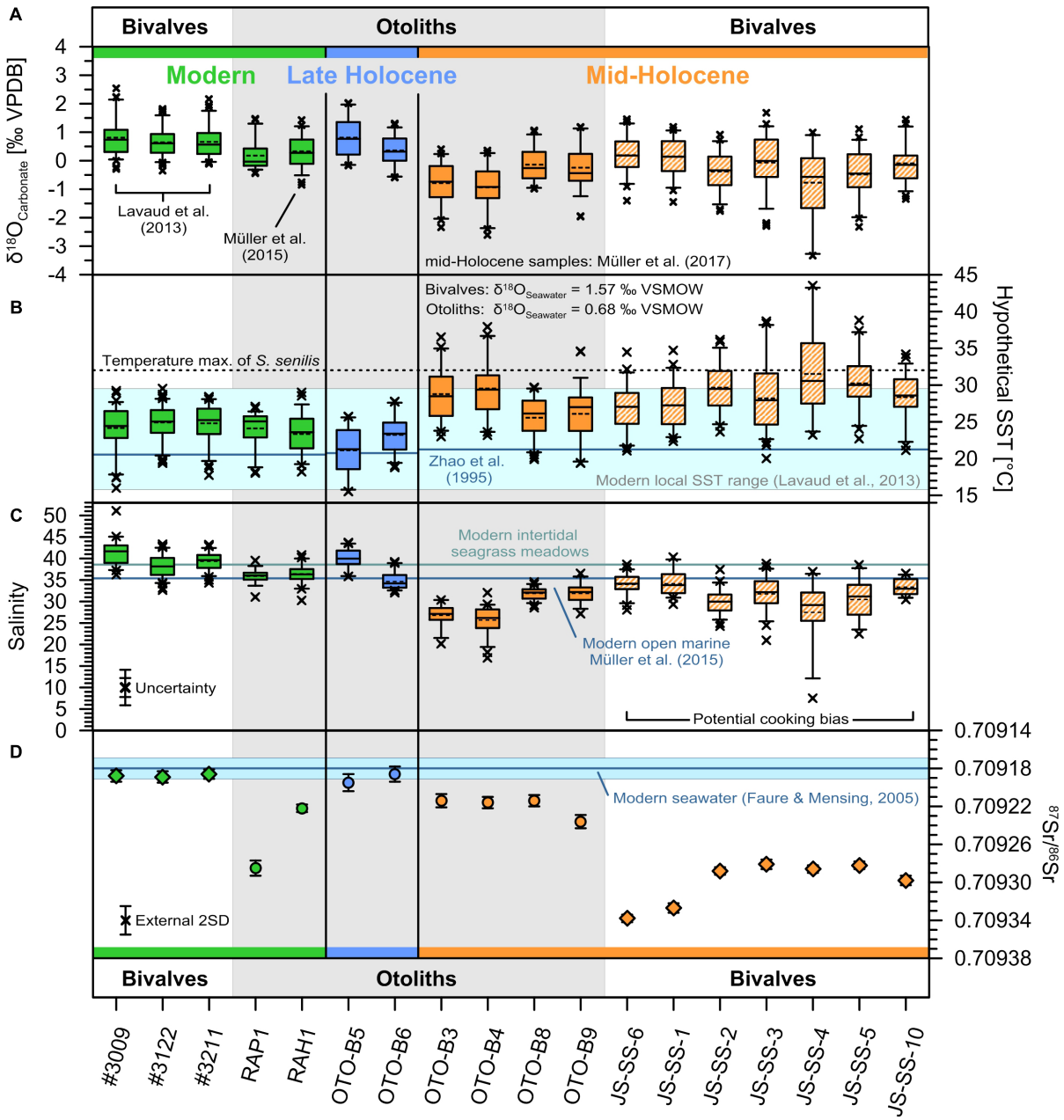


FIGURE 4 | Isotope records and proxy reconstructions of Mauritanian bivalve shells and otoliths. **(A)** Boxplot of measured bivalve shell and otolith $\delta^{18}O$ data (grey demarcation) from previously published modern *S. senilis* for Banc d'Arguin, Mauritania (Lavaud et al., 2013), and the modern *C. heudelotii* otolith record from the Banc d'Arguin (Müller et al., 2015). Modern (2010–2012 AD) samples are shown in green, late Holocene (ca. 3.0 ka BP) otolith samples in blue, and mid-Holocene (ca. 5.3–5.0 ka BP) samples in orange. Striated boxes of the mid-Holocene bivalves $\delta^{18}O$ data indicate potential minor alteration due to the exposure to prehistoric cooking methods prior to deposition (Müller et al., 2017). The box and whiskers represent the interquartile range and 5th/95th percentiles, respectively. The analytical uncertainty of the $\delta^{18}O$ analysis is smaller than the symbol size (±0.07‰ VPDB). Data points outside the whiskers represent statistical outliers. Solid and dotted horizontal lines inside the box show the median and average reconstructed water temperature values, respectively. **(B)** Boxplot of the hypothetical $\delta^{18}O$-derived SST assuming constant modern $\delta^{18}O_{Seawater}$ values with the modern seasonal water temperature range of the inner Banc d'Arguin from Lavaud et al. (2013) and the upper water temperature limit for *S. senilis* from Azzoug et al. (2012b) and the references therein for comparison. **(C)** Boxplot showing the reconstructed salinities using modern water temperature data and the different $\delta^{18}O_{Seawater}$-salinity relationships (**Figure 6**). The combined uncertainty includes the water temperature uncertainty of ±1°C (inner error bars) and the potential misalignment accounting for on average 1.15°C (outer error bars). Horizontal lines represent the average modern salinity of the open Banc d'Arguin of 36.7 S_p (Müller et al., 2015) and the intertidal areas in the eastern Banc d'Arguin of 40 S_p (Lavaud et al., 2013). **(D)** Bulk $^{87}Sr/^{86}Sr$ records of modern and Holocene carbonate samples. Note that the *y*-axis is inverted to facilitate comparisons between $^{87}Sr/^{86}Sr$ records and $\delta^{18}O$-based salinity reconstructions. Sample error bars for $^{87}Sr/^{86}Sr$ indicate two standard errors (SE) of the mean. The external instrumental uncertainty is given as 2SD (n = 263). The modern seawater composition of 0.70918 and corresponding 2SD (±0.00001) (Faure and Mensing, 2005) are indicated by the horizontal line and shading, respectively.

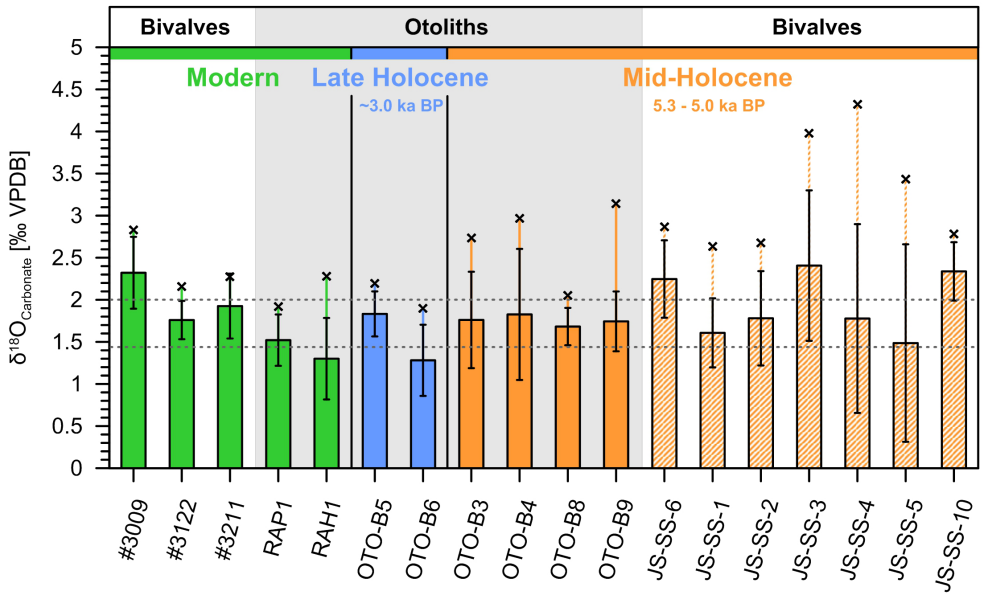


FIGURE 5 | Carbonate $\delta^{18}O$ seasonal amplitudes and ranges. Bars present the mean seasonal amplitude computed as the difference between the averages of all clearly distinguishable local minima and maxima in the raw ontogenetic $\delta^{18}O$ records of each sample (see **Supplementary Figures S2**, **S3**). Error bars indicate the propagated standard deviation (1SD). The horizontal dashed lines mark the modern mean values for bivalves (ca. 2.0‰) and otoliths (ca. 1.4‰). Black cross symbols above bars present the absolute range of values in a given record.

whose otoliths can hardly be distinguished in archaeological deposits, provide reliable records of environmental conditions experienced during the lifetime of the organism.

The late Holocene *Carlarius* spp. otoliths also show clear seasonal cycles within their ontogenetic $\delta^{18}O$ records (**Supplementary Figure S2**), with measured $\delta^{18}O$ values translating into water temperatures ranging from 15.5 to 27.8°C with average values of 21.1 and 23.3°C (**Figure 4B** and **Supplementary Figures S2**, **S4**). These hypothetical $\delta^{18}O$-based water temperatures are only slightly lower than those observed today. However, considering the uncertainty of modern otolith temperature reconstructions of $\leq \pm 1.16$°C (Müller et al., 2015), the late Holocene otolith $\delta^{18}O$-based water temperature reconstructions are in good agreement with alkenone-based SST estimates of the same period. The latter also indicate similar conditions in the mid-Holocene and present day (**Figure 2E**; Zhao et al., 1995; Kim et al., 2007). Therefore, the late Holocene *Carlarius* spp. otolith data do not show any evidence for isotopically lighter freshwater discharge, which in turn confirms previous studies that showed fully established arid conditions in most parts of NW Africa by ~3.0 ka BP (deMenocal et al., 2000; Kröpelin et al., 2008).

In contrast, mid-Holocene *S. senilis* shells exhibit $\delta^{18}O$ signatures that suggest ambient water temperatures between 20.0 and 43.5°C when assuming a constant $\delta^{18}O_{Seawater}$ value of +1.57‰ VSMOW (**Figure 4B**). However, alkenone-based temperatures during this period only ranged between 27.0 and 31.5°C (**Figure 2E**). Thus, the mid-Holocene *S. senilis* shells substantially overestimate modern seasonal water temperature minima and maxima by +6.1 and +7.7°C, respectively. Similarly, mid-Holocene otoliths show $\delta^{18}O_{Carbonate}$ values considerably lower than the modern and late Holocene specimens. In consequence, reconstructed water temperatures indicate average seasonal minimum and maximum water temperatures of ca. 21.4 and 34.7°C, which is +5.5 and +5.2°C warmer than observed today during the cold and warm season, respectively.

The clumped isotope analyses suggest that some of the *S. senilis* shells examined in this study may have been exposed to heat (prehistoric cooking) prior to deposition (Müller et al., 2017). This may have caused an alteration of their original $\delta^{18}O$ shell records towards lower isotopic values (i.e. higher reconstructed SSTs), mimicking the effect of elevated water temperatures or potential freshwater runoff (**Figure 3**). However, there is a robust agreement between potentially cooked (roasted) bivalve shells and the essentially pristine fish otoliths, suggesting that the initial $\delta^{18}O$ shell values remained effectively unchanged during any pre-depositional treatments. Importantly, even if assuming a pre-depositional alteration by heating, experimentally determined effects of different cooking practices on carbonate $\delta^{18}O$ values strongly suggest that the magnitude of modern water temperature overestimations by the ontogenetic $\delta^{18}O$ shell records are considerably larger than any expected cooking bias ($\leq$ 0.90‰ VPDB) (Müller et al., 2017). Based on the experimental findings, we are confident that any possible contributions of prehistoric cooking to the observed depletions in $\delta^{18}O$ shell values are limited and not decisive for our interpretations. Therefore, we conclude that the *S. senilis* $\delta^{18}O$ records still provide reliable palaeoenvironmental data from the mid-Holocene. Clumped isotopes of mid- and late Holocene fish otoliths are in turn largely coherent, and do not indicate

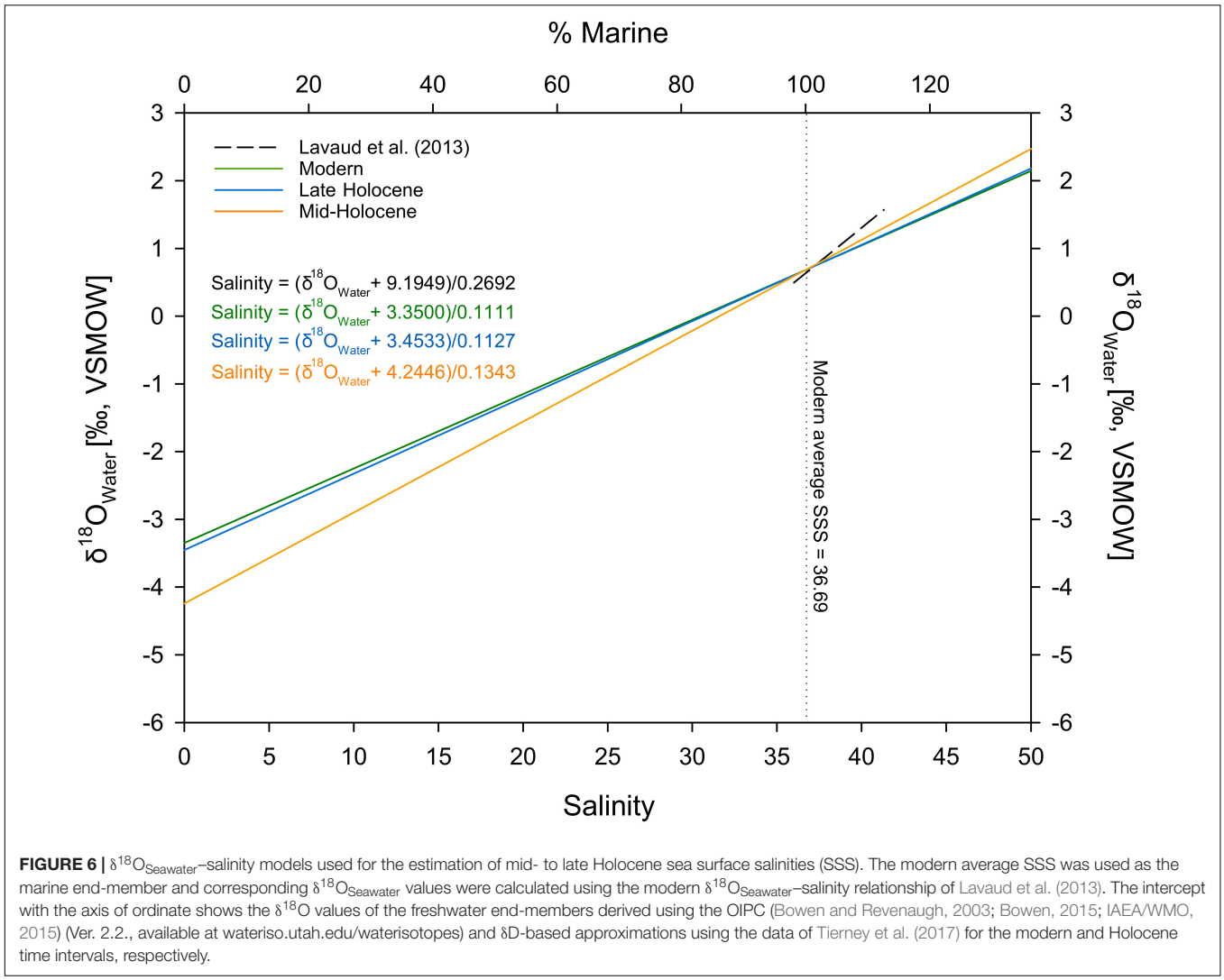


FIGURE 6 | $\delta^{18}O_{Seawater}$–salinity models used for the estimation of mid- to late Holocene sea surface salinities (SSS). The modern average SSS was used as the marine end-member and corresponding $\delta^{18}O_{Seawater}$ values were calculated using the modern $\delta^{18}O_{Seawater}$–salinity relationship of Lavaud et al. (2013). The intercept with the axis of ordinate shows the $\delta^{18}O$ values of the freshwater end-members derived using the OIPC (Bowen and Revenaugh, 2003; Bowen, 2015; IAEA/WMO, 2015) (Ver. 2.2., available at wateriso.utah.edu/waterisotopes) and δD-based approximations using the data of Tierney et al. (2017) for the modern and Holocene time intervals, respectively.

any significant effects of pre-depositional heating at higher temperatures by roasting or burning (> 170°C) that could introduce larger errors to $\delta^{18}O$-based water temperature and salinity reconstructions.

The consistently high mid-Holocene water temperature estimates found in several otoliths and bivalve shells are in strong opposition to different climate models (ca. +0.4 to +1.5°C) (Kim et al., 2007; Kutzbach and Liu, 1997) as well as marine palaeoclimate records from NW Africa for this time, which consistently indicate similar SSTs during the mid- to late Holocene as observed today (e.g. Zhao et al., 1995; Elderfield and Ganssen, 2000; Kim et al., 2007). Likewise, the foraminifera $\delta^{18}O$ record of the eastern tropical Atlantic was found to be rather stable during this period, indicating no major change in $\delta^{18}O_{Seawater}$ values during the mid- to late Holocene (Kim et al., 2007). However, it must be noted that a number of studies have suggested variable intensities of coastal upwelling off Mauritania during the Holocene, and some variability in water temperatures in response cannot be excluded. Pollen records from West Africa presented in Hély et al. (2014) indicate prolonged dry seasons and possibly associated intensified trade winds during the mid-Holocene that could have promoted upwelling along the Mauritanian coast (Talbot, 1981). However, along the inshore Banc d'Arguin corresponding to the location of the palaeo-estuary, satellite derived SST and nutrient data depict a notably limited influence of upwelling today (Carlier et al., 2015). A low input of upwelled water to the essentially sheltered inner Banc d'Arguin was further supported by N isotopic signatures in fish and their potential food sources, suggesting very limited supply of upwelled nutrients to inshore species (Carlier et al., 2015). Considering these observations, temperature variability is likely of lesser importance to the overall $\delta^{18}O$ composition of these waters in near-shore habitats, particularly for bivalves living within the palaeo-estuary.

Importantly, neither the relatively small variation in SST nor potential changes in $\delta^{18}O_{Seawater}$ values explain the high water temperatures found consistently among various skeletal components. Only shell gathering in intertidal pool environments with SSTs > 35°C by the Neolithic communities may have led to the strong overestimation of reasonable

water temperatures. However, the considerably lower maximal temperature tolerance of *S. senilis* of ∼32°C (Azzoug et al., 2012b), as well as the agreement of modern *S. senilis* shells with water temperature data from such intertidal environments (Lavaud et al., 2013), strongly suggest that this overestimation is most likely related to isotopically lighter freshwater discharge during the mid-Holocene.

Temporal differences are also reflected in the seasonality of raw ontogenetic $\delta^{18}O$ of samples from the different time periods, described here in terms of seasonal range and seasonal amplitude (**Figure 5**). Taking into account the distinct ecologies of studied taxa, mid-Holocene bivalve shells and catfish otoliths both have considerably higher ranges in their $\delta^{18}O$ records than their modern equivalents, whereas late Holocene otoliths are in turn consistent in this regard with modern specimens. Estimated mean seasonal amplitudes, however, are altogether less coherent with the assumption of a generally enhanced seasonal signal during the mid-Holocene. While mid-Holocene otolith samples show seasonal amplitudes consistently higher than the modern otolith average in line with pronounced seasonal discharge, mid-Holocene bivalve shell records vary considerably and generally depict a larger inter-annual variability than modern examples. However, discrepancies in the seasonal signatures of individual bivalves can be expected, given that the individual geographic location within the estuarine system plays a critical role in their exposure to discharge considering the (palaeo-)hydrology of the Banc d'Arguin (Barusseau et al., 2007). The large ranges of mid-Holocene shell records, on the other hand, support the presence of significant influx of isotopically lighter freshwater, although the latter may have not been strictly seasonally confined. Late Holocene otolith seasonal signals are consistent with modern records, which is in good agreement with the proposed lack of seasonal precipitation by ca. 3.0 ka BP.

In order to further constrain the potential influence of isotopically lighter freshwater runoff, and disentangle the origin of $\delta^{18}O_{Carbonate}$ values, we reconstructed ontogenetic salinity records under the assumption of comparable water temperatures during the mid-Holocene to those observed today. Based on different $\delta^{18}O_{Water}$-salinity models (**Figure 6**), the modern average reconstructed salinities are highly consistent with the measured values of ∼36 S_p for the otoliths (Müller et al., 2015) and ∼40 S_p for *S. senilis* shells (Lavaud et al., 2013) (**Figure 4C**). Similarly, essentially pure marine conditions are indicated by the late Holocene otoliths with salinities comparable to the modern value of ∼36 S_p. In the case of the mid-Holocene carbonate samples, however, the salinity reconstructions suggest consistently brackish to marine conditions within the coastal zones with average values between 25.7 and 31.8 S_p, and 27.5 and 34.1 S_p for the catfish otoliths and the bivalve shells, respectively. Regardless of the uncertainty of absolute salinity estimates (± ca. 4.1 S_p) due to unknown absolute water temperatures during the Holocene and potential temporal misalignments, the results thereby indicate lower salinities/$\delta^{18}O_{Seawater}$ at ∼5.2 ka BP that suggest considerable freshwater runoff even after the supposed aridification event at ∼5.5 ka BP.

Nonetheless, we note that the intra-shell salinity variations for the mid-Holocene shells range from relatively constant marine conditions (e.g. JS-SS-6, 1 and 10) to highly variable salinities, i.e. reflecting marine to brackish conditions (e.g. JS-SS-3, 4 and 5; **Figure 4C**). The fish otoliths, on the other hand, show remarkable differences with OTO-B3 and B4 indicating predominantly brackish conditions, whereas OTO-B8 and B9 suggest primarily near-marine salinities. While the salinity variations among the bivalve shells might be related to their spatial distribution within the estuarine mouth (i.e. high versus low salinity zones), the strong variation among the otoliths may suggest variable inter-annual discharge rates as a consequence of climate instability at ∼5.2 ka BP. However, the absence of clear freshwater-signals in individual samples does not necessarily exclude the persistence of monsoonal precipitation, but may be linked to the use of different gathering grounds by the respective coastal population across the estuary, and/or the ability of fish to move within the coastal zone. Moreover, it is important to note that the possibility of changes in the evaporative budget may present an additional control on observed oxygen isotopic signatures, and that Holocene salinity reconstructions may potentially be sensitive to non-intuitive variations in freshwater isotopic end-members linked to atmospheric processes (Leduc et al., 2013).

To complement ontogenetic $\delta^{18}O$ measurements, we further analysed bulk carbonate samples for Sr isotopes as a proxy for riverine Sr contributions into the coastal area of the Banc d'Arguin. In contrast to the $\delta^{18}O$ records, carbonate $^{87}Sr/^{86}Sr$ signatures are not sensitive to water temperature, and are little affected by kinetic fractionation. Thus, they present a means to further constrain the origin of observed $\delta^{18}O$ signals. The $^{87}Sr/^{86}Sr$ ratios of all mid-Holocene bivalve samples are considerably higher than the marine end-member of 0.70918 (**Figure 4D**), suggesting the presence of riverine discharge during the mid-Holocene. Despite a lack of modern reference values of terrestrial runoff along the Mauritanian coast, the consistently elevated ratios of bivalve shells are in good agreement with those of Sr sources expected to be drained during the AHP. Bedrock and derived soil or dust across NW Africa exhibit generally more radiogenic $^{87}Sr/^{86}Sr$ signatures relative to seawater (Scheuvens et al., 2013), and respective weathering products transported by runoff can be assumed to show similar isotopic ratios. Indeed, recent evidence suggests that the mobilisation of weathering products may have been significantly amplified by increasing human activity and associated land-use for grazing during the mid- to late Holocene (Wright, 2017; Zerboni and Nicoll, 2019). Regardless, the $^{87}Sr/^{86}Sr$ ratios are highly consistent amongst different bivalve samples, suggesting similar degrees of exposure to a non-marine Sr source during their lifetime (**Figure 4D**).

Similarly, otoliths from the mid-Holocene also depict a coherent, although not as pronounced deviation from the seawater composition. This offset relative to bivalve shells from this period may be linked to differences between the taxa and their respective mobility. For example, *Carlarius* spp. are exposed to purely marine conditions during their reproductive stage, but may also move between preferred habitats throughout their lifetime regardless of maturity, whereas bivalves are sessile. In contrast, the late Holocene otoliths show $^{87}Sr/^{86}Sr$ ratios

indistinguishable from those of seawater. This is in good agreement with $\delta^{18}O$-based salinity reconstructions that suggest a lack of significant freshwater influx by this time. Arid conditions are well reflected in modern bivalve shells, whose $^{87}Sr/^{86}Sr$ signatures consistently depict marine values. $^{87}Sr/^{86}Sr$ signatures of modern catfish otoliths exhibit unexpected deviations from the seawater end-member, as well as inconsistencies among samples. Considering that there is virtually no freshwater discharge to the Banc d'Arguin today, the origin of the modern otolith $^{87}Sr/^{86}Sr$ signatures is unclear. One potential source of non-marine strontium may be provided by anthropogenic inputs (e.g. sewage). These inputs can locally alter the natural Sr isotopic composition of water (Böhlke and Horan, 2000) and the catfish may have been exposed when dwelling close to townships along the shallow eastern Baie du Lévrier. The ingestion of radiogenic sediments due to the bottom feeding of catfish may further contribute to the observed Sr isotopic signatures, although the dietary contribution of Sr to otoliths is likely inconsequential (Walther and Thorrold, 2006), and comparable $^{87}Sr/^{86}Sr$ anomalies are absent in late Holocene specimens. We considered the possibility of diagenetic alterations to the observed $^{87}Sr/^{86}Sr$ signatures (see for example Marcano et al., 2015), and the influence of contamination by detrital matter to be minimal based on initial treatments and investigations. Despite the inconsistencies in $^{87}Sr/^{86}Sr$ in modern catfish otoliths, we consider the Holocene records to be reliable and reflective of the presence and absence of terrestrial runoff to the Banc d'Arguin in the mid- and late Holocene, respectively. This is further supported by their generally good agreement with the $\delta^{18}O$ proxy records, the environmental controls of which are distinctly different and independent from those governing $^{87}Sr/^{86}Sr$ signatures in water. $^{87}Sr/^{86}Sr$ values of dissolved Sr, which is incorporated into otoliths and bivalve shells without considerable isotopic fractionation, are not affected by water temperature or evaporation (Doebbert et al., 2014). While observed $\delta^{18}O$ records may to some extent be influenced by variations in water temperature and/or local evaporative regimes, the consistently elevated $^{87}Sr/^{86}Sr$ signatures of mid-Holocene samples can be expected to be unaffected by such changes. Our Sr isotope data thus support the assumption that $\delta^{18}O$ records can be interpreted primarily in terms of local salinity variations in response to terrestrial discharge of freshwater, rather than changes in water temperature or the evaporation budget.

Altogether, our bivalve shell and otolith records thereby depict mid-Holocene freshwater runoff that is likely indicative of persistent, but possibly ceasing monsoonal activity across large parts of NW Africa between ca. 5.0 and 5.3 ka BP. Furthermore, our records confirm the establishment of the modern arid state by ∼3.0 ka BP, corresponding largely to continental records and archaeological evidence for this region (Cremaschi et al., 2006; Kröpelin et al., 2008).

CONCLUSION

By providing strong evidence for isotopically lighter monsoon discharge at ∼5.2 ka BP at ∼20.5°N, our data support the hypothesis of a prolonged transitional termination of the AHP with a likely gradual aridification of the coastal zones along the Banc d'Arguin during the mid-Holocene, and the establishment of arid conditions by ∼3.0 ka BP. The $^{87}Sr/^{86}Sr$ analyses largely agree with $\delta^{18}O$-based salinity estimations, and provide additional indications for significant precipitation across the NW African hinterland after the suggested abrupt aridification event around 5.5 ka BP. Our data are consistent with the precipitation reconstructions of Tierney et al. (2017), which also indicate the persistence of considerable rainfall until ∼3–4 ka BP. Moreover, our record is coherent with the local occupation history in the Ras el Sass area that was abandoned at ∼3 ka BP, most likely as a consequence of decreasing surface freshwater availability (Vernet and Tous, 2004). On a broader scale, our data support the concept of a temporally and spatially heterogeneous aridification of NW Africa throughout the mid- to late Holocene as indicated by various continental records and archaeological sequences (Kröpelin et al., 2008; Lézine et al., 2011). The abrupt increase of dust export at ∼5.5 ka BP may, however, indicate the onset of a general aridification trend across NW Africa, but the likely integration over a large dust source area may have masked regional deviations from this overall climatic shift. Nevertheless, our data show that arid conditions were established at ∼20.5°N by ∼3.0 ka BP. Finally, the vast successions of shell middens along the Banc d'Arguin allow for the establishment of highly resolved records of Holocene climate variability and thereby provide a valuable means to further constrain the nature and timing of the AHP termination.

DATA AVAILABILITY STATEMENT

The datasets analysed for this study can be found at PANGAEA®, Data Publisher for Earth & Environmental Science, https://doi.pangaea.de/10.1594/PANGAEA.889705.

AUTHOR CONTRIBUTIONS

PM and HW designed the research. PM and SH completed the sampling and sample analysis. PM, SH, and HCW completed the data analysis and interpretations, and served as primary authors. FL, SK, and SH carried out the Sr-isotope analysis. J-PB and RV recovered the shell samples and were responsible for local logistics, archaeological expertise, and permitting in Mauritania. All authors discussed the results and wrote the manuscript.

FUNDING

Funding for this study was provided by the Leibniz Centre for Tropical Marine Research (ZMT), Bremen, Germany. Sr analyses were additionally financed through the project "New Regional Formations," kindly supported by the VolkswagenStiftung, Hanover, Germany, and its funding line "Key Issues for Research and Society."

ACKNOWLEDGMENTS

We thank the following people for their assistance and support: Romain Lavaud and Julien Thébault for providing the modern bivalve samples; Philippe Tous for providing modern otolith samples; Peter K. Swart, Philip T. Staudigel, and Sean. T. Murray (RSMAS, University of Miami) for clumped isotope analysis assistance; Sebastian Flotow (ZMT) for sample preparation; Henning Kuhnert (University of Bremen) and Dorothee Dasbach (ZMT) for oxygen isotope analysis; Christoph Vogt (University of Bremen) for help with XRD analysis; SCALGOlive (www.scalgo.com) for providing the modern catchment area data; Janna Just for informative comments and suggestions; Matthias López-Correa and André Klicpera for helpful discussions; and the reviewers for constructive criticisms and helpful suggestions to improve this manuscript.

SUPPLEMENTARY MATERIAL

The Supplementary Material for this article can be found online at: https://www.frontiersin.org/articles/10.3389/feart.2019.00314/full#supplementary-material

REFERENCES

Affek, H. P., and Eiler, J. M. (2006). Abundance of mass 47 CO_2 in urban air, car exhaust, and human breath. *Geochim. Cosmochim. Acta* 70, 1–12. doi: 10.1016/j.gca.2005.08.021

Andrus, C. F. T., and Crowe, D. E. (2002). Alteration of otolith aragonite: effects of prehistoric cooking methods on otolith chemistry. *J. Archaeol. Sci.* 29, 291–299. doi: 10.1006/jasc.2001.0694

Armitage, S. J., Bristow, C. S., and Drake, N. A. (2015). West African monsoon dynamics inferred from abrupt fluctuations of Lake Mega-Chad. *Proc. Natl. Acad. Sci. U.S.A.* 112, 8543–8548. doi: 10.1073/pnas.1417655112

Azzoug, M., Carré, M., Chase, B. M., Deme, A., Lazar, A., Lazareth, C. E., et al. (2012a). Positive precipitation-evaporation budget from AD 460 to 1090 in the Saloum Delta (Senegal) indicated by mollusk oxygen isotopes. *Glob. Planet. Change* 9, 54–62. doi: 10.1016/j.gloplacha.2012.08.003

Azzoug, M., Carré, M., and Schauer, A. J. (2012b). Reconstructing the duration of the West African monsoon season from growth patterns and isotopic signals of shells of *Anadara senilis* (Saloum Delta, Senegal). *Palaeogeogr. Palaeoclimatol. Palaeoecol.* 346–347, 145–152. doi: 10.1016/j.palaeo.2012.06.001

Barusseau, J.-P., Vernet, R., Saliège, J.-F., and Descamps, C. (2007). Late Holocene sedimentary forcing and human settlements in the Jerf el Oustani - Ras el Sass = Occupation humaine et forçages sédimentaires à l'Holocène final dans la région de Jerf el Oustani - Ras el Sass (Banc d'Arguin, Mauritanie). *Géomorphol. Reli. Process. Environ.* 7, 17–28. doi: 10.4000/geomorphologie.634

Bloszies, C., Forman, S. L., and Wright, D. K. (2015). Water level history for Lake Turkana, Kenya in the past 15,000 years and a variable transition from the African Humid Period to Holocene aridity. *Glob. Planet. Change* 132, 64–76. doi: 10.1016/j.gloplacha.2015.06.006

Böhlke, J. K., and Horan, M. (2000). Strontium isotope geochemistry of groundwaters and streams affected by agriculture, Locust Grove, MD. *Appl. Geochem.* 15, 599–609. doi: 10.1016/S0883-2927(99)00075-X

Bougeois, L., de Rafélis, M., Reichart, G. J., de Nooijer, L. J., Nicollin, F., and Dupont-Nivet, G. (2014). A high resolution study of trace elements and stable isotopes in oyster shells to estimate Central Asian Middle Eocene seasonality. *Chem. Geol.* 363, 200–212. doi: 10.1016/j.chemgeo.2013.10.037

Bowen, G. J. (2015). *The Online Isotopes in Precipitation Calculator, version 2.2*. Available at: wateriso.utah.edu/waterisotopes (accessed December, 2008).

Bowen, G. J., and Revenaugh, J. (2003). Interpolating the isotopic composition of modern meteoric precipitation. *Water Resour. Res.* 39:1299. doi: 10.1029/2003WR002086

Brahim, K. (2004). *Ecologie et Biologie de L'émissole Lisse Mustelus Mustelus (Linné, 1758) Sur Les Côtes de Mauritanie*. Brest: Thèse Université de Bretagne Occidentale.

Bronk Ramsey, C. (1995). Radiocarbon calibration and analysis of stratigraphy: the OxCal program. *Radiocarbon* 37, 425–430. doi: 10.1017/S0033822200030903

Carlier, A., Chauvaud, L., van der Geest, M., Le Loc'h, F., Le Duff, M., Vernet, M., et al. (2015). Trophic connectivity between offshore upwelling and the inshore food web of Banc d'Arguin (Mauritania): new insights from isotopic analysis. *Estuar. Coast. Shelf Sci.* 165, 149–158. doi: 10.1016/j.ecss.2015.05.001

Carton, J. A., and Giese, B. S. (2008). A reanalysis of ocean climate using simple ocean data assimilation (SODA). *Mon. Weather Rev.* 136, 2999–3017. doi: 10.1175/2007MWR1978.1

Castañeda, I. S., Schouten, S., Pätzold, J., Lucassen, F., Kasemann, S., Kuhlmann, H., et al. (2016). Hydroclimate variability in the Nile River Basin during the past 28,000 years. *Earth Planet. Sci. Lett.* 438, 47–56. doi: 10.1016/j.epsl.2015.12.014

Claussen, M., Bathiany, S., Brovkin, V., and Kleinen, T. (2013). Simulated climate-vegetation interaction in semi-arid regions affected by plant diversity. *Nat. Geosci.* 6, 954–958. doi: 10.1038/ngeo1962

Collins, J. A., Prange, M., Caley, T., Gimeno, L., Beckmann, B., Mulitza, S., et al. (2017). Rapid termination of the African Humid Period triggered by northern high-latitude cooling. *Nat. Commun.* 8:1372. doi: 10.1038/s41467-017-01454-y

Craig, H. (1961). Isotopic variations in meteoric waters. *Science* 133, 1702–1703. doi: 10.1126/science.133.3465.1702

Cremaschi, M., Pelfini, M., and Santilli, M. (2006). Cupressus dupreziana: a dendroclimatic record for the middle-late Holocene in the central Sahara. *Holocene* 16, 293–303. doi: 10.1191/0959683606hl926rr

Cremaschi, M., and Zerboni, A. (2009). Early to middle Holocene landscape exploitation in a drying environment: two case studies compared from the central Sahara (SW Fezzan, Libya). *Comptes Rendus Geosci.* 341, 689–702. doi: 10.1016/j.crte.2009.05.001

Cremaschi, M., Zerboni, A., Charpentier, V., Crassard, R., Isola, I., Regattieri, E., et al. (2015). Early-Middle Holocene environmental changes and pre-Neolithic human occupations as recorded in the cavities of Jebel Qara (Dhofar, southern Sultanate of Oman). *Quat. Int.* 382, 264–276. doi: 10.1016/j.quaint.2014.12.058

deMenocal, P. B., Ortiz, J., Guilderson, T., Adkins, J., Sarnthein, M., Baker, L., et al. (2000). Abrupt onset and termination of the African Humid Period: rapid climate responses to gradual insolation forcing. *Quat. Sci.* 19, 347–361. doi: 10.1016/s0277-3791(99)00081-5

Deniel, C., and Pin, C. (2001). Single-stage method for the simultaneous isolation of lead and strontium from silicate samples for isotopic measurements. *Anal. Chim. Acta* 426, 95–103. doi: 10.1016/S0003-2670(00)01185-1185

Dennis, K. J., Affek, H. P., Passey, B. H., Schrag, D. P., and Eiler, J. M. (2011). Defining an absolute reference frame for "clumped" isotope studies of CO_2. *Geochim. Cosmochim. Acta* 75, 7117–7131. doi: 10.1016/j.gca.2011.09.025

Doebbert, A. C., Johnson, C. M., Carroll, A. R., Beard, B. L., Pietras, J. T., Rhodes Carson, M., et al. (2014). Controls on Sr isotopic evolution in lacustrine systems: Eocene green river formation. *Wyo. Chem. Geol.* 380, 172–189. doi: 10.1016/j.chemgeo.2014.04.008

Elderfield, H., and Ganssen, G. (2000). Past temperature and $\delta^{18}O$ of surface ocean waters inferred from foraminiferal Mg/Ca ratios. *Nature* 405, 442–445. doi: 10.1038/35013033

Faure, G., and Mensing, T. M. (2005). *Isotopes : Principles and Applications*, 3rd Edn. Hoboken, NJ: wiley.

Gonfiantini, R., Stichler, W., and Rozanski, K. (1995). "Standards and intercomparison materials distributed by the International Atomic Energy Agency for stable isotope measurements," in *Proceedings of the Consultants Meeting on Reference and Intercomparison Materials for Stable Isotopes of Light Elements*, (Vienna: IAEA), 13–29.

Goodwin, D. H., Schöne, B. R., and Dettman, D. L. (2003). Resolution and fidelity of oxygen isotopes as paleotemperature proxies in bivalve mollusk shells:

models and observations. *Palaios* 18, 110–125. doi: 10.1669/0883-1351(2003)18<110:rafooi>2.0.co;2

Grossman, E. L., and Ku, T.-L. (1986). Oxygen and carbon isotope fractionation in biogenic aragonite: temperature effects. *Chem. Geol. Isot. Geosci. Sect.* 59, 59–74. doi: 10.1016/0168-9622(86)90057-90056

Hanebuth, T. J. J., and Henrich, R. (2009). Recurrent decadal-scale dust events over Holocene western Africa and their control on canyon turbidite activity (Mauritania). *Quat. Sci. Rev.* 28, 261–270. doi: 10.1016/j.quascirev.2008.09.024

Hély, C., Lézine, A. M., Ballouche, A., Cour, P., Duzer, D., Guinet, P., et al. (2014). Holocene changes in African vegetation: tradeoff between climate and water availability. *Clim. Past* 10, 681–686. doi: 10.5194/cp-10-681-2014

Holz, C., Stuut, J. B. W., Henrich, R., and Meggers, H. (2007). Variability in terrigenous sedimentation processes off northwest Africa and its relation to climate changes: inferences from grain-size distributions of a Holocene marine sediment record. *Sediment. Geol.* 202, 499–508. doi: 10.1016/j.sedgeo.2007.03.015

Huntington, K. W., Eiler, J. M., Affek, H. P., Guo, W., Bonifacie, M., Yeung, L. Y., et al. (2009). Methods and limitations of 'clumped' CO_2 isotope ($\Delta 47$) analysis by gas-source isotope ratio mass spectrometry. *J. Mass Spectrom.* 44, 1318–1329. doi: 10.1002/jms.1614

IAEA/WMO, (2015). *Global Network of Isotopes in Precipitation*. Vienna: IAEA.

Kim, J.-H., Meggers, H., Rimbu, N., Lohmann, G., Freudenthal, T., Müller, P. J., et al. (2007). Impacts of the North Atlantic gyre circulation on Holocene climate off northwest Africa. *Geology* 35, 387–390. doi: 10.1130/G23251A.1

Kröpelin, S., Verschuren, D., Lézine, A. M., Eggermont, H., Cocquyt, C., Francus, P., et al. (2008). Climate-driven ecosystem succession in the Sahara: the past 6000 years. *Science* 320, 765–768. doi: 10.1126/science.1154913

Kuhlmann, H., Meggers, H., Freudenthal, T., and Wefer, G. (2004). The transition of the monsoonal and the N Atlantic climate system off NW Africa during the Holocene. *Geophys. Res. Lett.* 31:L22204. doi: 10.1029/2004GL021267

Kuper, R., and Kröpelin, S. (2006). Climate-controlled Holocene occupation in the Sahara: motor of Africa's evolution. *Science* 313, 803–807. doi: 10.1126/science.1130989

Kutzbach, J. E., and Liu, Z. (1997). Response of the African monsoon to orbital forcing and ocean feedbacks in the middle Holocene. *Science* 278, 440–443. doi: 10.1126/science.278.5337.440

Laskar, J., Robutel, P., Joutel, F., Gastineau, M., Correia, A. C. M., and Levrard, B. (2004). A long-term numerical solution for the insolation quantities of the Earth. *Astron. Astrophys.* 428, 261–285. doi: 10.1051/0004-6361, 20041335

Lavaud, R., Thébault, J., Lorrain, A., van der Geest, M., and Chauvaud, L. (2013). *Senilia senilis* (Linnaeus, 1758), a biogenic archive of environmental conditions on the Banc d'Arguin (Mauritania). *J. Sea Res.* 76, 61–72. doi: 10.1016/j.seares.2012.11.003

Leduc, G., Sachs, J. P., Kawka, O. E., and Schneider, R. R. (2013). Holocene changes in eastern equatorial Atlantic salinity as estimated by water isotopologues. *Earth Planet. Sci. Lett.* 362, 151–162. doi: 10.1016/j.epsl.2012.12.003

Lehner, B., Verdin, K., and Jarvis, A. (2008). New global hydrography derived from spaceborne elevation data. *Eos Trans. Am. Geophys. Union* 89, 93–94. doi: 10.1029/2008EO100001

Lézine, A. M. (2009). Timing of vegetation changes at the end of the Holocene humid period in desert areas at the northern edge of the Atlantic and Indian monsoon systems. *Comptes Rendus Geosci.* 341, 750–759. doi: 10.1016/j.crte.2009.01.001

Lézine, A. M., Zheng, W., Braconnot, P., and Krinner, G. (2011). Late Holocene plant and climate evolution at Lake Yoa, northern Chad: pollen data and climate simulations. *Clim. Past* 7, 1351–1362. doi: 10.5194/cp-7-1351-2011

Lindauer, S., Milano, S., Steinhof, A., and Hinderer, M. (2018). Heating mollusc shells – A radiocarbon and microstructure perspective from archaeological shells recovered from Kalba, Sharjah Emirate, UAE. *J. Archaeol. Sci. Rep.* 21, 528–537. doi: 10.1016/j.jasrep.2018.08.041

Liu, Z., Wang, Y., Gallimore, R., Gasse, F., Johnson, T., deMenocal, P., et al. (2007). Simulating the transient evolution and abrupt change of Northern Africa atmosphere-ocean-terrestrial ecosystem in the Holocene. *Quat. Sci. Rev.* 26, 1818–1837. doi: 10.1016/j.quascirev.2007.03.002

Marcano, M. C., Frank, T. D., Mukasa, S. B., Lohmann, K. C., and Taviani, M. (2015). Diagenetic incorporation of Sr into aragonitic bivalve shells: implications for chronostratigraphic and palaeoenvironmental interpretations. *Depos. Rec.* 1, 38–52. doi: 10.1007/BF01530197

Maritan, L., Mazzoli, C., and Freestone, I. (2007). Modelling changes in mollusc shell internal microstructure during firing: implications for temperature estimation in shell-bearing pottery. *Archaeometry* 49, 529–541. doi: 10.1111/j.1475-4754.2007.00318.x

McGee, D., deMenocal, P. B., Winckler, G., Stuut, J.-B. W., and Bradtmiller, L. I. (2013). The magnitude, timing and abruptness of changes in North African dust deposition over the last 20,000 yr. *Earth Planet. Sci. Lett.* 37, 163–176. doi: 10.1016/j.epsl.2013.03.054

Milano, S., and Nehrke, G. (2018). Microstructures in relation to temperature-induced aragonite-to-calcite transformation in the marine gastropod *Phorcus turbinatus*. *PLoS One* 13:e0204577. doi: 10.1371/journal.pone.0204577

Milano, S., Prendergast, A. L., and Schöne, B. R. (2016). Effects of cooking on mollusk shell structure and chemistry: implications for archeology and paleoenvironmental reconstruction. *J. Archaeol. Sci. Rep.* 7, 14–26. doi: 10.1016/j.jasrep.2016.03.045

Mokadem, F., Parkinson, I. J., Hathorne, E. C., Anand, P., Allen, J. T., and Burton, K. W. (2015). High-precision radiogenic strontium isotope measurements of the modern and glacial ocean: limits on glacial-interglacial variations in continental weathering. *Earth Planet. Sci. Lett.* 415, 111–120. doi: 10.1016/j.epsl.2015.01.036

Müller, P., Staudigel, P. T., Murray, S. T., Vernet, R., Barusseau, J.-P., Westphal, H., et al. (2017). Prehistoric cooking versus accurate palaeotemperature records in shell midden constituents. *Sci. Rep.* 7:3555. doi: 10.1038/s41598-017-03715-3718

Müller, P., Taylor, M. H., Klicpera, A., Wu, H. C., Michel, J., and Westphal, H. (2015). Food for thought: mathematical approaches for the conversion of high-resolution sclerochronological oxygen isotope records into sub-annually resolved time series. *Palaeogeogr. Palaeoclimatol. Palaeoecol.* 440, 763–776. doi: 10.1016/j.palaeo.2015.09.032

Palmer, M. R., and Edmond, J. M. (1989). The strontium isotope budget of the modern ocean. *Earth Planet. Sci. Lett.* 92, 11–26. doi: 10.1016/0012-821X(89)90017-90014

Pausata, F. S. R., Messori, G., and Zhang, Q. (2016). Impacts of dust reduction on the northward expansion of the African monsoon during the Green Sahara period. *Earth Planet. Sci. Lett.* 434, 298–307. doi: 10.1016/j.epsl.2015.11.049

Rachmayani, R., Prange, M., and Schulz, M. (2015). North African vegetation-precipitation feedback in early and mid-Holocene climate simulations with CCSM3-DGVM. *Clim. Past* 11, 175–185. doi: 10.5194/cp-11-175-2015

Reimer, P. J., Bard, E., Bayliss, A., Beck, J. W., Blackwell, P. G., Ramsey, C. B., et al. (2013). IntCal13 and marine13 radiocarbon age calibration curves 0-50,000 years cal BP. *Radiocarbon* 55, 1869–1887. doi: 10.2458/azu-js-rc.55.16947

Ritchie, J. C., Eyles, C. H., and Haynes, C. V. (1985). Sediment and pollen evidence for an early to mid-Holocene humid period in the eastern Sahara. *Nature* 314, 352–355. doi: 10.1038/314352a0

Roberts, N. (2014). *The Holocene – An Environmental History*. 3rd Edn. Blackwell: Wiley.

Romero, O. E., Kim, J.-H., and Donner, B. (2008). Submillennial-to-millennial variability of diatom production off Mauritania, NW Africa, during the last glacial cycle. *Paleoceanography* 23:A3218. doi: 10.1029/2008PA001601

Scheuvens, D., Schütz, L., Kandler, K., Ebert, M., and Weinbruch, S. (2013). Bulk composition of northern African dust and its source sediments - A compilation. *Earth Sci. Rev.* 116, 170–194. doi: 10.1016/j.earscirev.2012.08.005

Shanahan, T. M., McKay, N. P., Hughen, K. A., Overpeck, J. T., Otto-Bliesner, B., Heil, C. W., et al. (2015). The time-transgressive termination of the African Humid Period. *Nat. Geosci.* 8, 140–144. doi: 10.1038/ngeo2329

Skonieczny, C., Paillou, P., Bory, A., Bayon, G., Biscara, L., Crosta, X., et al. (2015). African humid periods triggered the reactivation of a large river system in Western Sahara. *Nat. Commun.* 6, 6–11. doi: 10.1038/ncomms9751

Surge, D., and Walker, K. J. (2005). Oxygen isotope composition of modern and archaeological otoliths from the estuarine hardhead catfish (*Ariopsis felis*) and their potential to record low-latitude climate change. *Palaeogeogr. Palaeoclimatol. Palaeoecol.* 228, 179–191. doi: 10.1016/j.palaeo.2005.03.051

Talbot, M. R. (1981). Holocene changes in tropical wind intensity and rainfall: evidence from southeast Ghana. *Quat. Res.* 16, 201–220. doi: 10.1016/0033-5894(81)90045-90044

Thorrold, S. R., Campana, S. E., Jones, C. M., and Swart, P. K. (1997). Factors determining $\delta^{13}C$ and $\delta^{18}O$ fractionation in aragonitic otoliths of marine fish.

Geochim. Cosmochim. Acta 61, 2909–2919. doi: 10.1016/S0016-7037(97)00141-145

Tierney, J. E., Pausata, F. S. R., and deMenocal, P. B. (2017). Rainfall regimes of the Green Sahara. *Sci. Adv.* 3:e1601503. doi: 10.1126/sciadv.1601503

Tjallingii, R., Claussen, M., Stuut, J.-B. W., Fohlmeister, J., Jahn, A., Bickert, T., et al. (2008). Coherent high- and low-latitude control of the northwest African hydrological balance. *Nat. Geosci.* 1, 670–676. doi: 10.1038/ngeo289

USGS, (2004). *Shuttle Radar Topography Mission, 1 Arc Second scene SRTM_u03_n008e004, Unfilled Unfinished 2.0. Global Land Cover Facility*. College Park, MD: University of Maryland.

Vernet, R. (2007). *Le golfe d'Arguin de la Préhistoire à L'histoire Littoral et Plaines Intérieures*. Nouakchott: Parc National du Banc d'Arguin.

Vernet, R., and Tous, P. (2004). Les amas coquilliers de Mauritanie occidentale et leur contexte paléoenvironnemental (VIIe-IIe millénaires BP). *Préhistoire Anthropol. Méditerranéennes* 13, 55–69.

Walther, B., and Thorrold, S. (2006). Water, not food, contributes the majority of strontium and barium deposited in the otoliths of a marine fish. *Mar. Ecol. Prog. Ser.* 311, 125–130. doi: 10.3354/meps311125

Wright, D. K. (2017). Humans as agents in the termination of the African Humid Period. *Front. Earth Sci.* 5:1–14. doi: 10.3389/feart.2017.00004

Zerboni, A., and Nicoll, K. (2019). Enhanced zoogeomorphological processes in North Africa in the human-impacted landscapes of the Anthropocene. *Geomorphology* 331, 22–35. doi: 10.1016/j.geomorph.2018.10.011

Zhao, M., Beveridge, N. A. S., Shackleton, N. J., Sarnthein, M., and Eglinton, G. (1995). Molecular stratigraphy of cores off northwest Africa: sea surface temperature history over the last 80 Ka. *Paleoceanography* 10, 661–675. doi: 10.1029/94PA03354

Zhao, W., Balsam, W., Williams, E., Long, X., and Ji, J. (2018). Sr-Nd-Hf isotopic fingerprinting of transatlantic dust derived from North Africa. *Earth Planet. Sci. Lett.* 486, 23–31. doi: 10.1016/j.epsl.2018.01.004

Conflict of Interest: The authors declare that the research was conducted in the absence of any commercial or financial relationships that could be construed as a potential conflict of interest.

Copyright © 2019 Höpker, Wu, Müller, Barusseau, Vernet, Lucassen, Kasemann and Westphal. This is an open-access article distributed under the terms of the Creative Commons Attribution License (CC BY). The use, distribution or reproduction in other forums is permitted, provided the original author(s) and the copyright owner(s) are credited and that the original publication in this journal is cited, in accordance with accepted academic practice. No use, distribution or reproduction is permitted which does not comply with these terms.